

基于响应面法和遗传神经网络模型的高沉积率激光熔覆参数优化

庞伟帆, 傅戈雁*, 王明雨, 龚燕琪, 余司琪, 徐加超, 刘凡

苏州大学机电工程学院激光制造技术研究所, 江苏 苏州 215021

摘要 在大功率激光熔覆成形中, 熔覆层的沉积率是决定成形效率及质量等的重要因素。采用 Box-Behnken (BBD) 及正交法进行了激光熔覆单道沉积实验设计, 研究了激光功率、送粉速率、扫描速度和离焦量对沉积率的关系。分别建立了响应面法 (RSM) 模型和经遗传算法优化的神经网络 (GA-BP) 模型, 同时预测并优化了沉积工艺参数。经遗传神经网络模型优化后的工艺参数得到的最大沉积率为 61.74 g/min, 高于响应面法优化得到的 53.55 g/min。结果表明, 遗传神经网络模型的预测、泛化及优化能力要优于响应面法模型, 使用遗传算法优化后的神经网络模型可为实现高沉积率激光熔覆成形提供更有效的预估方法。

关键词 激光加工; 激光熔覆; 沉积率优化; 响应面; 遗传算法; 神经网络

中图分类号 TN249

文献标志码 A

doi: 10.3788/CJL202148.0602112

1 引言

激光熔覆快速成形技术是近年来逐渐发展起来的一种先进制造技术, 广泛应用于高性能、具有复杂结构的金属零件的无模具快速成形^[1-3]。传统的金属激光快速成形大多在低于 2000 W 的小功率条件下进行, 成形时间长, 成形效率低, 材料利用不充分^[4-6], 成形过程对每层熔覆层的沉积速率及成形质量有很高的要求。而采用大功率中空环形激光进行熔覆, 通过优化实验参数, 能有效提高成形效率。同时, 采用光内送粉的方式, 粉末与光同轴送出且被光包围, 粉末充分进入熔池, 光粉耦合较好。目前针对激光熔覆沉积效率的研究主要是以单因素实验或正交实验为依据, 定性地研究工艺参数的影响。由于工艺参数对熔覆沉积率的关系是非线性的, 故很难通过简单的参数模型来表述。

近年来, 神经网络模型已经广泛应用于各个学科领域。神经网络预测模型无须预先指定函数形式, 通过迭代学习对非线性数据进行拟合和建模, 有强大的处理多元非线性问题的能力^[7-9], 能够解决多

个工艺参数耦合对目标的影响, 在激光熔覆、激光焊接和激光通信等方面有广阔的应用前景。苏州大学蒋伟伟等^[10]使用二次回归和神经网络模型建立了激光熔覆参数与熔覆层几何特征的预测模型。刘立君等^[11]运用 BP (back propagation) 神经网络反求激光熔凝参数, 误差可以控制在 3% 以内。Rahimi 等^[12]将响应面法 (RSM) 和神经网络结合, 建立模型, 优化了在 Al-SiC 复合材料上进行激光雕刻的工艺参数。传统神经网络收敛速度慢, 初始权值与阈值均为随机值, 容易陷入局部最优解, 产生的误差较大。此外, 在激光快速成形过程中, 激光熔覆头、送粉器等设备及外界因素的变化会造成最佳工艺参数的改变, 因此需提供在固定实验设备及外界条件下完成确定工艺目标所对应的工艺参数。

本文采用中空环形光内送粉喷头, 在工艺范围内设计了四因素三水平正交实验, 在正交实验的基础上分析成形过程中工艺参数对熔覆层单道沉积速率的关系。通过在工艺区间内设计 Box-Behnken (BBD) 实验及随机参数实验, 建立响应曲面模型和遗传神经网络模型, 对比两种模型的预测能力并优

收稿日期: 2020-06-22; 修回日期: 2020-07-23; 录用日期: 2020-09-24

基金项目: 国家重点研发计划(2017YFB1103601)

* E-mail: fugeyan@suda.edu.cn

化工艺参数。本研究可作为闭环控制过程中的估计器,在加工过程中不断调整工艺参数,可为实现高沉积率激光熔覆成形提供一定的参考。

2 实验准备

2.1 实验系统

实验设备为中空环形光内送粉熔覆系统,主要包括 6 kW Raycus 激光器、6 轴 KUKA 机器人、中空环形光内送粉喷头、GTV 高精度载气送粉器、制氮系统等。中空环形光内送粉喷头在焦点处的直径为 3 mm,其光强分布可表示为

$$I(r,0) = \begin{cases} I' \exp\left(-K \cdot \frac{r^2}{R_0^2}\right), & |r| \geq r' \\ 0, & 0 \leq |r| < r' \end{cases}, \quad (1)$$

式中: I' 为环形光圈光强; r 为所测点到光斑中心的距离; R_0 为光斑半径; r' 为中空环形光圈半径; K 为常数。送粉喷头在三维方向的移动由 KUKA 机器人控制,在流量为 80 L/min 的氮气保护下,沉积扫描长度为 40 mm 的单层熔覆层。图 1 和图 2 所示为光内送粉原理图及实验设备。

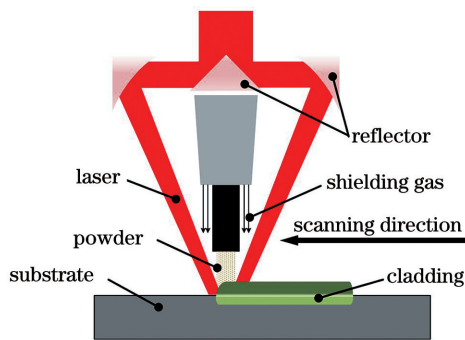


图 1 光内送粉激光熔覆原理图

Fig. 1 Schematic diagram of laser cladding with powder feeding

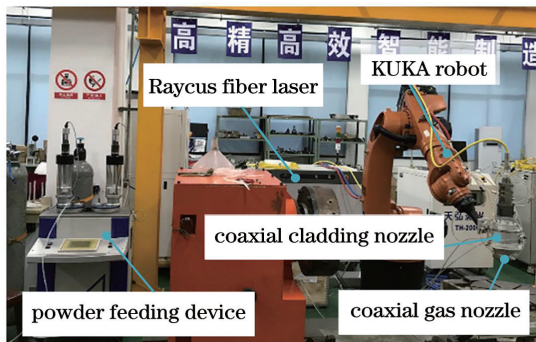


图 2 实验设备图

Fig. 2 Diagram of experimental equipment

2.2 实验材料及样本准备

实验采用基材为 304 不锈钢,尺寸为 150 mm×150 mm×10 mm。粉末为 Fe314 铁基合金粉末,粉末粒度为 45~109 μm,其材料成分如表 1 所示。

表 1 Fe314 合金成分表

Table 1 Composition of Fe314 powder unit: %

Element	Fe	C	Cr	B	Si	Ni
Mass fraction	Bal.	0.1	15.0	1.0	1.0	1.0

熔覆前对基体表面用无水乙醇或丙酮进行除污,然后与粉末一起烘干备用。实验完成后,将处理好的样品放入到精密天平中,称重后得到单道沉积质量(g/min),以计算熔道沉积率 R_d (g/min),再将不同沉积率试样沿熔道截面方向切割后进行磨样、抛光、腐蚀,用电镜观察组织形貌,得到熔道截面示意图,如图 3 所示。其中,沉积率是单位时间内沉积的粉末质量。截面形状不变且熔道稳定的理想状态下,沉积率计算公式为

$$R_d = \frac{m}{t} = \frac{\rho S l}{l/v} = \rho S v, \quad (2)$$

式中: ρ 为沉积合金密度; S 为熔覆层截面积; v 为扫描速度。实际实验中,可采用称重法获得每条熔道的质量,此时沉积率计算公式为

$$R_d = \frac{m}{t} = \frac{m}{l/v}, \quad (3)$$

式中: m 为沉积单道质量; l 为扫描长度。

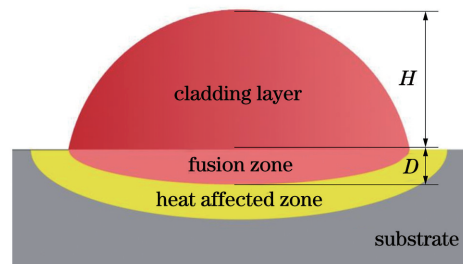


图 3 熔道截面示意图

Fig. 3 Schematic diagram of weld passage section

2.3 实验设计及分析

激光快速成形技术中熔覆层沉积率的影响因素比较复杂,其中激光功率(P)、送粉速率(v_f)、扫描速度(v_s)、离焦量(D)这 4 个工艺参数对熔覆层的形成影响较为显著。为了研究各工艺参数对单道熔覆层沉积率(R_d)的影响规律,采用四因素三水平的正交实验法进行实验设计,确定激光功率(P)、送粉速率(v_f)、扫描速度(v_s)、离焦量(D)这 4 个工艺参数对单道熔覆层沉积率的影响,并观察低沉积率与高沉积率样品显微组织的差异,正交实验的工艺区

间及实验参数和结果 $L_9(3^4)$ 见表 2。

表 2 正交实验参数及结果

Table 2 Orthogonal experimental parameters and results

No.	P/W	$v_f/$ ($g \cdot min^{-1}$)	$v_s/$ ($mm \cdot s^{-1}$)	$D/$ mm	$R_d/$ ($g \cdot min^{-1}$)
1	3200	43.5	8	-10	27.6
2	3200	58.0	10	-11	49.5
3	3200	72.5	12	-12	57.6
4	3500	72.5	10	-10	66.0
5	3500	58.0	8	-12	44.4
6	3500	43.5	12	-11	36.0
7	4000	43.5	10	-12	42.0
8	4000	58.0	12	-10	55.8
9	4000	72.5	8	-11	68.4

正交实验采用极差分析法进行分析,实验评价指标为单道沉积率,对表 2 实验结果进行分析,结果如表 3 所示,表中: K_i 表示与因素 i 对应的水平三次实验的平均值; η 为极差,即因素极大值与极小值之差。结果表明,送粉速率对熔覆沉积率的影响最大,其次是激光功率及扫描速度,离焦量对熔覆沉积速率的影响最小。由于在激光功率与扫描速度一定的情况下,单位时间内粉末和基体所吸收的能量一

表 3 正交实验极差分析结果

Table 3 Orthogonal experimental range analysis results

Parameter	P/W	$v_f/(g \cdot min^{-1})$	$v_s/(mm \cdot s^{-1})$	D/mm
K_1	44.9	35.2	46.8	49.8
K_2	48.8	49.9	52.5	51.3
K_3	55.4	64.0	49.8	48.0
η	10.5	28.8	5.7	3.3

表 4 BBD 实验参数及结果

Table 4 BBD experimental parameters and results

Experiment	P/W	$v_f/(g \cdot min^{-1})$	$v_s/(mm \cdot s^{-1})$	D/mm	$R_d/(g \cdot min^{-1})$	Cladding morphology
(1)	3200	58.0	12	-11	39.6	
(2)	3200	43.5	10	-11	28.5	
(3)	3200	72.5	10	-11	54.0	
(4)	3200	58.0	8	-11	43.2	
(5)	3200	58.0	10	-12	39.0	
(6)	3200	58.0	10	-10	39.0	

定,因此送粉速率增加,进入激光照射区域的粉末量增加,熔化的粉末增多,熔覆层变高,沉积率变大。而离焦量的大小影响熔池热耦合区域的大小,即熔池宽度,进而影响沉积率。

对低沉积率及高沉积率样品进行镶样、打磨、腐蚀,用电子扫描显微镜(SEM)观察熔覆层下部对应组织,如图 4 所示。

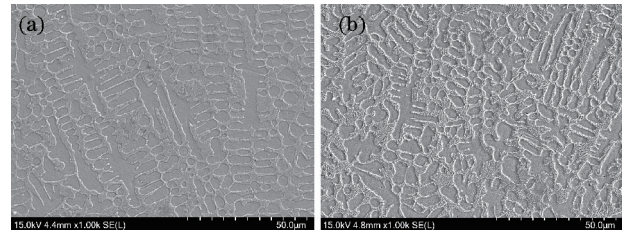


图 4 不同沉积率激光熔覆 Fe314 合金显微组织。

(a)1 号样本; (b)9 号样本

Fig. 4 Microstructure of laser cladding Fe314 with different deposition rates. (a) Sample 1; (b) sample 9

由图 4 可见,在不同沉积率下,熔道组织均为外延生长的柱状枝晶。其中,在高沉积率下,由于送粉速率增大导致基体吸收激光能量减小,熔覆材料熔融温度较低,熔覆层组织细化,界面初生柱状晶生长能力减弱,故图 4(b)中晶粒略小于图 4(a),但两种沉积率组织均无明显的裂纹、孔隙等缺陷。

RSM 模型是一种解决多变量问题的统计方法,模型的建立采用 BBD 设计实验,Box-Behnken 是一种由 2^k 析因设计(k 为因子个数)和不完全区组设计组合而成的拟合响应曲面的三水平设计方法。该方法有利于减少实验次数,适用于大量组合试验分析和因素非线性影响研究^[13-14]。因此,在工艺区间内,通过 Design-Expert 10 的响应面模块进行 BBD 实验设计,生成了 29 组数据,对 29 组数据进行 29 组单道熔覆实验,表 4 为实验设计和结果。

Experiment	P / W	$v_t / (\text{g} \cdot \text{min}^{-1})$	$v_s / (\text{mm} \cdot \text{s}^{-1})$	D / mm	$R_d / (\text{g} \cdot \text{min}^{-1})$	Cladding morphology	
(7)	3600	43.5	12	-11	34.2		
(8)	3600	58.0	10	-11	51.0		
(9)	3600	58.0	10	-11	52.5		
(10)	3600	72.5	8	-11	63.6		
(11)	3600	43.5	8	-11	28.8		
(12)	3600	72.5	10	-12	55.5		
(13)	3600	43.5	10	-10	33.0		
(14)	3600	58.0	12	-10	46.8		
(15)	3600	58.0	8	-10	50.4		
(16)	3600	58.0	8	-12	46.8		
(17)	3600	58.0	10	-11	49.5		
(18)	3600	72.5	12	-11	46.8		
(19)	3600	58.0	10	-11	52.5		
(20)	3600	43.5	10	-12	28.5		
(21)	3600	58.0	10	-11	46.5		
(22)	3600	72.5	10	-10	61.5		
(23)	3600	58.0	12	-12	48.6		
(24)	4000	58.0	10	-10	57.0		
(25)	4000	58.0	8	-11	57.6		
(26)	4000	58.0	12	-11	52.2		
(27)	4000	72.5	10	-11	69.0		
(28)	4000	58.0	10	-12	46.5		
(29)	4000	43.5	10	-11	31.5		


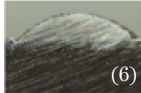
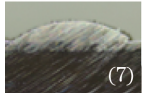

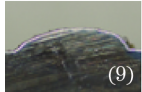
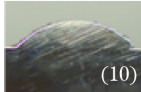
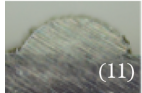

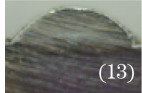



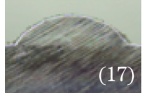


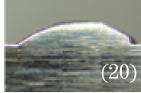
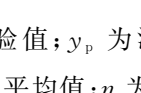
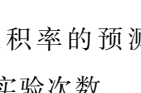
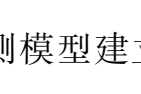

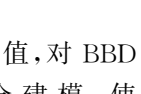
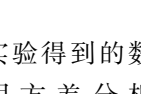
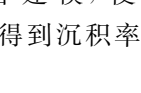
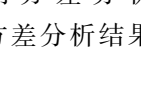

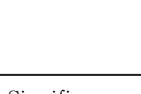
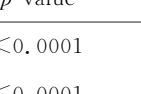
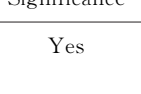




因建立神经网络预测模型需要大量实验样本,而经上述实验设计获得的 38 组样本满足不了模型的训练要求,故在工艺区间内用 MATLAB 随

机生成 20 组实验来添加样本数量,以使训练出的模型具有一定的泛化能力。实验设计和结果如表 5 所示。

表 5 随机参数实验参数及结果

Table 5 Random parameter experimental parameters and results

Experiment	P / W	$v_t / (\text{g} \cdot \text{min}^{-1})$	$v_s / (\text{mm} \cdot \text{s}^{-1})$	D / mm	$R_d / (\text{g} \cdot \text{min}^{-1})$	Cladding morphology	
(1)	4000	43.5	9.0	-10.5	37.8		
(2)	3600	46.4	11.0	-11.0	33.0		
(3)	3500	49.3	9.5	-12.0	38.5		
(4)	3300	49.3	9.0	-10.0	39.1		

Experiment	P / W	$v_f / (g \cdot \text{min}^{-1})$	$v_s / (\text{mm} \cdot \text{s}^{-1})$	D / mm	$R_d / (g \cdot \text{min}^{-1})$	Cladding morphology	
(5)	3900	49.3	12.0	-12.0	39.6		
(6)	4000	52.2	11.0	-10.0	44.5		
(7)	3800	55.1	12.0	-11.5	45.0		
(8)	3600	58.0	9.0	-11.5	39.1		
(9)	3700	60.9	11.5	-12.0	41.4		
(10)	3800	63.8	9.0	-12.0	41.8		
(11)	3600	66.7	8.5	-11.0	45.9		
(12)	3900	66.7	9.0	-12.0	40.5		
(13)	4000	66.7	8.5	-11.0	44.6		
(14)	3800	66.7	11.0	-11.5	47.8		
(15)	3900	66.7	11.5	-10.0	55.2		
(16)	3700	66.7	11.5	-12.0	46.6		
(17)	3800	69.6	9.0	-10.5	48.6		
(18)	3700	69.6	8.0	-11.0	45.6		
(19)	3600	72.5	11.5	-10.5	58.6		
(20)	3200	72.5	10.0	-12.0	42.0		

实验以均方根误差 (RMSE)、绝对平均偏差 (AAD) 评价模型精度及稳定性。RMSE 和 AAD 越低, 表明模型精度和稳定性越好。运用 AAD 对比 RSM 和 GA-BP 两种模型预测的沉积率值, RMSE 和 AAD 的表达式为

$$R_{MSE} = \sqrt{\left[\frac{1}{n} \sum_{i=1}^n (y_p - y_e)^2 \right]}, \quad (4)$$

$$\Delta_{AAD} = \left[\frac{1}{n} \sum_{i=1}^n (|y_e - y_p| / \bar{y}_e) \right] \times 100\%, \quad (5)$$

表 6 基于 RSM 模型预测的沉积率方差分析

Table 6 Analysis of variance of deposition rate predicted by RSM model

Source	Sum of squares	Mean square	F value	p value	Significance
Model	3069.27	383.66	45.49	<0.0001	Yes
A-P	414.19	414.19	49.11	<0.0001	
B- v_f	2293.57	2293.57	271.97	<0.0001	
C- v_s	41.07	41.07	4.87	0.0392	
D-D	43.32	43.32	5.14	0.0347	
AB	36.00	36.00	4.27	0.0520	
AD	27.56	27.56	3.27	0.0857	
BC	123.21	123.21	14.61	0.0011	

式中, y_e 为沉积率的实验值; y_p 为沉积率的预测值; \bar{y}_e 为沉积率实验值的平均值; n 为实验次数。

3 熔覆沉积率预测模型建立

3.1 RSM 模型建立

以沉积率 R_d 为响应值, 对 BBD 实验得到的数据进行多元回归拟合建模, 使用方差分析 (ANOVA) 法分析模型, 得到沉积率方差分析结果如表 6 所示。

Source	Sum of squares	Mean square	F value	p value	Significance
B ²	90.35	90.35	10.71	0.0038	
Residual	168.67	8.43			
Lack of fit	143.47	8.97	1.42	0.3985	No
Pure error	25.20	6.30			

在表 6 中, F 值表示 F 检验的统计量值, 失拟项 p 值表示因素的显著性程度, 由表可知: 激光功率(A)及送粉速度(B)对沉积率的影响极为显著 ($p < 0.0001$), 扫描速度(C)及离焦量(D)对沉积率的影响较为显著 ($p < 0.05$); 通过比较均方值的大小可知, 影响沉积率大小的工艺参数主次排序为 $B > A > D > C$; 方程二次项中 B^2 为较显著因素, 其余均不显著; 各交互项中 BC 为较显著因素, 其余均

不显著。表中失拟项的 p 值为 0.3985 ($p > 0.05$), 失拟项不显著, 这说明该模型可以较好地描述激光熔覆沉积率与各因素之间的关系。

此外, RSM 模型的总离差值为 3237.93, 决定系数 R^2 值为 0.9479, R^2_{adjust} 值为 0.9271, 经过 (4) 式和 (5) 式计算, 均方根误差为 2.4117、绝对平均偏差为 3.57%, 最终的响应回归预测二次多项式模型建立如下:

$$R_d = -17.0460 \times 10^{-3} v_f^2 + 5.1724 \times 10^{-4} P \cdot v_f + 6.5625 \times 10^{-3} P \cdot D - 0.1914 v_f \cdot v_s + 0.0569 P + 2.9825 v_f + 10.1750 v_s - 21.7250 D - 350.0824. \quad (6)$$

3.2 RSM 模型工艺参数交互性分析

基于多元回归方程及方差分析, 绘出各实验因素交互影响的三维曲面图, 由图 5 可以直观反映出激光功率、扫描速度、送粉速度与离焦量及其交互作用对沉积率的影响。其中, 随着激光功率(A)的增加, 激光能量密度增大, 熔池高温区范围增大, 在一定的功率范围内, 沉积率随着熔池熔化粉末的增多而显著提高, 即送粉速度和激光功率共同影响沉积率的大小, 如图 5(a) 所示。而随着负离焦(D)从 10 mm 增大到 12 mm 时, 光斑中空直径从 2 mm

增大到 3 mm, 光斑中心能量密度低, 粉末并未得到充分熔化。在功率变化不大的情况下, 粉末进入熔池熔化的数量并没有明显上升, 因此沉积率变化不明显, 如图 5(b) 所示。而随着送粉速度(B)的增加和扫描速度(C)的降低, 沉积率明显增加, 如图 5(c) 所示。这是由于较大的送粉速度和较慢的扫描速度导致基体粉末在单位时间内能获得较多的能量, 粉末得到充分熔化, 形成的熔覆层高度较高, 熔覆层饱满, 沉积率高, 因而这两种因素的交互作用最为显著。

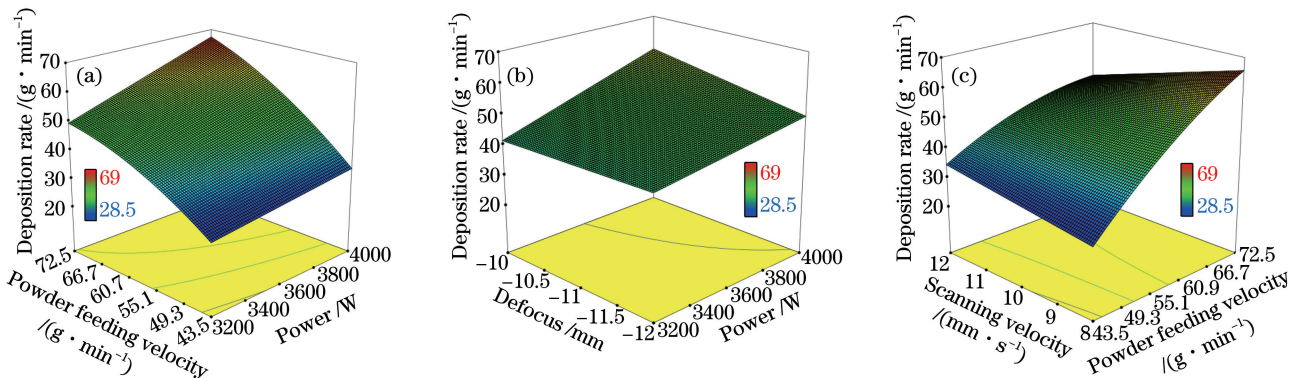


图 5 工艺参数对沉积速率的交互影响。(a) 送粉速率和激光功率; (b) 离焦量和激光功率; (c) 扫描速率和送粉速率

Fig. 5 Interactive influence of process parameters on deposition rate. (a) Powder feeding velocity and power; (b) defocus and power; (c) scanning velocity and powder feeding velocity

3.3 基于遗传算法优化的神经网络模型建立

BP 神经网络是一种由输入层、隐藏层、输出层

组成的多层前馈神经网络^[15]。遗传算法(GA)是一种模拟自然界遗传机制和达尔文生物进化论时形成

的一种并行随机搜索算法,能同时处理多个个体,适合进行多参数实时优化^[16]。用遗传算法对 BP 神经网络进行优化,将 BP 神经网络训练得到误差作为适应度值,获取最优初始权值与阈值,构建基于遗传算法优化的 BP 神经网络模型,图 6 为模型结构拓扑图,其中 ω_{ij} 及 ω_{jk} 为权值矩阵。

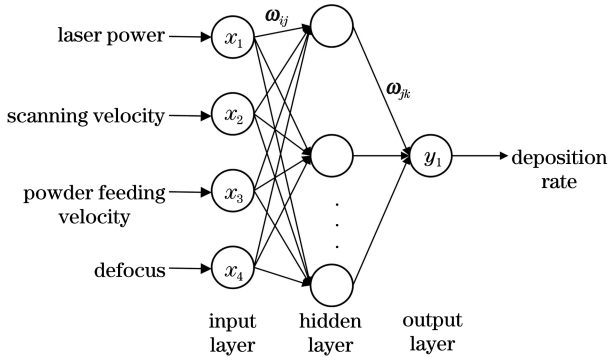


图 6 BP 神经网络拓扑结构

Fig. 6 Topological structure of BP neural network

基于前面实验设计中制备的 58 组样本,随机取其中的 75% 作为训练样本,其余 25% 作为测试样本。在 GA-BP 模型中,输入层选取 4 个神经元,分别输入激光功率、送粉速率、扫描速度、离焦量。选用双隐含层神经网络模型,神经元数可先分别试取

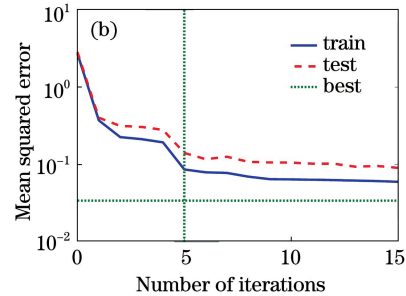
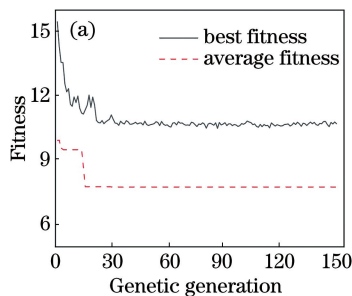


图 7 误差迭代图。(a) 遗传适应度进化;(b) 神经网络误差迭代

Fig. 7 Diagrams of error iteration. (a) Evolution of genetic fitness; (b) iteration of neural network error

训练完成后,遗传神经网络模型的决定系数 R^2 值为 0.9726,经过 (4) 式和 (5) 式计算得出 GA-BP 的 RMSE 和 AAD 分别为 1.8247 和 3.47%。

3.4 RSM 与 GA-BP 模型对比

基于实验设计的 RSM 和 GA-BP 模型对激光熔覆沉积率进行回归分析,图 8 给出了两种模型的实验预测值的对比分析图,由图可知两种模型均具有较好的拟合精度,但 GA-BP 的决定系数 R^2 更接近于 1,因此 GA-BP 模型具有更高的稳定性。通过比较两个模型的 RMSE 和 AAD 值可以发现,在激光熔覆沉积率多变量耦合分析中,GA-BP 的建模能力更强。

4 和 3,之后进行模型的调参更改。因此,神经网络的结构为 $4 \times 4 \times 3 \times 1$ 。在网络训练前,通过遗传算法计算适应度值来获取神经网络最优权值阈值,其中适应度计算函数 f 为

$$f = |y(x) - o(x)|, \quad (7)$$

式中: $y(x)$ 为 BP 神经网络的期望输出; $o(x)$ 为预测输出。设定遗传算法种群规模为 60,进化次数为 150 次,交叉概率为 0.65,变异概率为 0.025,得到最优个体。把遗传算法得到的最优个体赋值给 BP 神经网络,用该网络进行样本的训练与预测。设定初始网络参数的迭代次数为 5000 次,学习率为 0.025,训练目标为 0.00001。通过调参直至样本验证集的网络预测精度达 90%,训练完成后对其预测能力进行评估。

采用上述方法,在 MATLAB 软件中进行编程,建立激光熔覆单道沉积率预测模型。遗传适应度进化图和 BP 神经网络训练误差迭代图如图 7 所示,可以看出当种群遗传到 150 代时,适应度数值达到 7.79,把遗传算法优化后得到的初始权值和阈值赋值给 BP 神经网络进行学习更新,当迭代到第 15 代后,训练集的均方差为 0.0341,达到了所设定的训练目标。

为了对比 RSM 和 GA-BP 模型的泛化能力,通过 MATLAB 在工艺范围内随机生成 10 组工艺参数进行单道沉积率实验,实验结果及两种模型预测结果如图 9 中所示。根据方程计算得出 RSM 和 GA-BP 的 AAD 值分别为 8.762%、4.938%。因此,GA-BP 模型对预测沉积率有更强的泛化能力和预测精度。

为了对比两种模型对沉积率的优化效果,在熔覆层连续完整、球化和波纹状较少的情况下使沉积速率达到最优,以 BBD 实验及正交实验结果作为沉积率范围,在 28.5~69.0 g/min 范围内设置沉积率的目标值为最大。

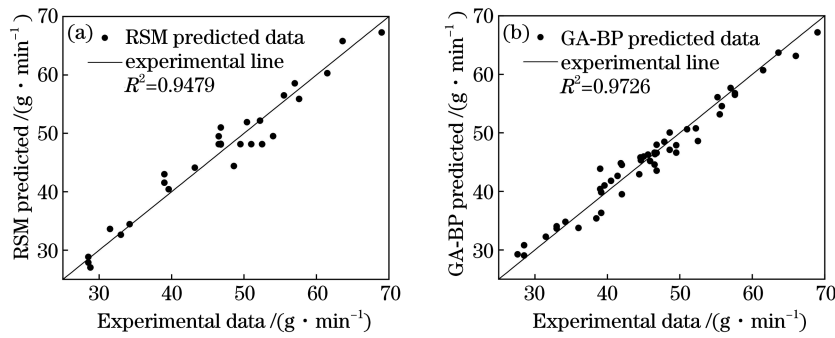


图 8 RSM 和 GA-BP 模型的预测对比结果。(a) RSM 模型;(b) GA-BP 模型

Fig. 8 Predicted comparison results of RSM and GA-BP models. (a) Model of RSM; (b) model of GA-BP

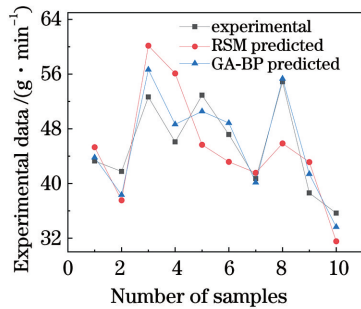



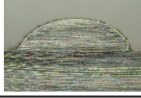
图 9 RSM 和 GA-BP 泛化能力比较

Fig. 9 Comparison of RSM and GA-BP generalization ability

RSM 模型经过优化后最终得到最佳工艺参数为:激光功率为 3600 W,送粉速度为 72.5 g/min,扫描速度为 8.5 mm/s,离焦量为 -11.7 mm,此时理论沉积率为 69.40 g/min。在此条件下进行单道熔覆实验,重复 3 次,沉积率取平均值为 53.55 g/min,

表 7 RSM 和 GA-BP 优化结果比较

Table 7 Comparison of optimization results between RSM and GA-BP

Optimization method	P / W	$v_t / (g \cdot \min^{-1})$	$v_s / (mm \cdot s^{-1})$	D / mm	Experimental $R_d / (g \cdot \min^{-1})$	Theoretical $R_d / (g \cdot \min^{-1})$	Error / %	Cladding morphology
RSM	3600	72.5	8.5	-11.7	53.55	69.40	29.6	
GA-BP	3720	72.5	9.6	-10	61.74	59.89	3.0	

4 结 论

基于中空环形光内送粉熔覆系统,在正交实验的基础上,采用 BBD 实验设计进行实验,建立了以沉积率为响应目标的 RSM 模型,研究了激光功率、送粉速度、扫描速率和离焦量及两种重要因素交互对大功率激光熔覆沉积率的影响。同时,基于上述实验及随机参数实验建立 GA-BP 模型,对两种模型的建模和泛化能力进行了分析及对比,并对激

与理论值相差 29.6%。

GA-BP 模型通过 BP 神经网络模型调试遗传的适应度,以沉积率作为函数的输出值,用遗传算法进行多变量全局寻优,获取最高沉积率 59.89 g/min 的工艺参数为:激光功率为 4000 W,送粉速度为 72.5 g/min,扫描速度为 9.8 mm/s,离焦量为 -10 mm。在此工艺参数下进行单道熔覆实验,重复 3 次,沉积率取平均值为 61.74 g/min,实验值与预测值相差 3.0%。

从表 7 可以看出,GA-BP 优化实验得到的沉积率 61.74 g/min 高于 RSM 模型优化实验得到的沉积率 53.55 g/min,且 GA-BP 预测的准确率要高于 RSM,这表明在相同送粉速率下,经遗传算法寻优后的沉积率比 RSM 更高,该模型对大功率激光熔覆沉积更有实际意义。

光熔覆高沉积率的工艺条件进行了优化,对比两种模型的性能及优化结果,得出以下结论:

GA-BP 模型的均方根误差和绝对平均偏差均比 RSM 模型要小,RSM 模型和 GA-BP 模型的决定系数分别为 0.9479 和 0.9726,这表明 GA-BP 模型的评估性能要略优于 RSM 模型。

GA-BP 模型和 RSM 模型预测能力很接近,但针对激光熔覆高沉积率进行优化时,寻优的最佳沉积率为 61.74 g/min,高于 RSM 模型优化得到的

53.55 g/min。因此,GA-BP 模型是优化获得高熔覆沉积率的一种有效方法,模型可靠性高,能搜索出特定工艺范围内最优沉积率,可作为后闭环控制高效高沉积率成形实体件的估计器。

参 考 文 献

- [1] Shi Y S. Laser manufacturing technology [M]. Beijing: China Machine Press, 2012: 42-262.
史玉升. 激光制造技术[M]. 北京: 机械工业出版社, 2012: 42-262.
- [2] Li D S, Shi T, Shi S H, et al. Laser cladding forming technology of flat-top thin-walled part based on special-shaped base surface[J]. Chinese Journal of Lasers, 2019, 46(11): 1102002.
李东升, 石拓, 石世宏, 等. 异形基面平顶薄壁结构激光熔覆成形工艺研究[J]. 中国激光, 2019, 46(11): 1102002.
- [3] Ocelik V, Nenadl O, Palavra A, et al. On the geometry of coating layers formed by overlap [J]. Surface and Coatings Technology, 2014, 242: 54-61.
- [4] Wang H M. Materials' fundamental issues of laser additive manufacturing for high-performance large metallic components [J]. Acta Aeronautica et Astronautica Sinica, 2014, 35(10): 2690-2698.
王华明. 高性能大型金属构件激光增材制造: 若干材料基础问题[J]. 航空学报, 2014, 35(10): 2690-2698.
- [5] Huang J S, Shi S H, Sun C F. The existing state of rapid prototyping by large power laser accurately cladding metal powder[J]. Journal of Suzhou Institute of Silk Textile Technology, 2005, 25(4): 16-18.
黄家胜, 石世宏, 孙承峰. 大功率激光精密熔覆金属粉末快速成形技术发展现状[J]. 苏州大学学报(工科版), 2005, 25(4): 16-18.
- [6] Li Z, Sui S, Yuan Z H, et al. Microstructure and tensile properties of high-deposition-rate laser metal deposited GH4169 alloy [J]. Chinese Journal of Lasers, 2019, 46(1): 0102004.
李祚, 隋尚, 袁子豪, 等. 高沉积率激光熔覆沉积 GH4169 合金的微观组织与拉伸性能[J]. 中国激光, 2019, 46(1): 0102004.
- [7] Dong C H. MATLAB neural network and application [M]. Beijing: National Defense Industry Press, 2005.
董长虹. Matlab 神经网络与应用[M]. 北京: 国防工业出版社, 2005.
- [8] Li Y H, Liu P, Zhou J B, et al. Center extraction of structured light stripe based on back propagation neural network [J]. Acta Optica Sinica, 2019, 39(12): 1212005.
李玥华, 刘朋, 周京博, 等. 基于 BP 神经网络的结构光光条中心提取[J]. 光学学报, 2019, 39(12): 1212005.
- [9] Zhang M Y, Liang Y M. Color Fourier ptychography microscopy using three-dimensional convolutional neural network [J]. Acta Optica Sinica, 2020, 40(20): 2011001.
张慕阳, 梁艳梅. 基于三维卷积神经网络的彩色傅里叶叠层显微术[J]. 光学学报, 2020, 40(20): 2011001.
- [10] Jiang W W, Fu G Y, Zhang J P, et al. Prediction of geometrical shape of coaxial wire feeding cladding in three-beam [J]. Infrared and Laser Engineering, 2020, 49(3): 0305005.
蒋伟伟, 傅戈雁, 张吉平, 等. 三分光束光内同轴送丝熔覆层几何形貌预测[J]. 红外与激光工程, 2020, 49(3): 0305005.
- [11] Liu L J, Jiang Y Q, Wang X P, et al. Inverse solution of BP neural network for laser remelting parameters [J]. Journal of Harbin University of Science and Technology, 2017, 22(3): 112-116.
刘立君, 姜亚青, 王晓鹏, 等. 激光熔凝参数 BP 神经网络的反求[J]. 哈尔滨理工大学学报, 2017, 22(3): 112-116.
- [12] Rahimi M H, Shayganmanesh M, Noorossana R, et al. Modelling and optimization of laser engraving qualitative characteristics of Al-SiC composite using response surface methodology and artificial neural networks [J]. Optics & Laser Technology, 2019, 112: 65-76.
- [13] Yan R, Li H, Li J C, et al. Process parameters optimization of polystyrene powder selective laser sintering based on response surface methodology [J]. Chinese Journal of Lasers, 2019, 46(3): 0302015.
鄢然, 李浩, 李军超, 等. 基于响应面法的聚苯乙烯粉末选择性激光烧结成型工艺参数优化[J]. 中国激光, 2019, 46(3): 0302015.
- [14] Gong Y Q, Fu G Y, Shi T, et al. Research on local atmosphere protection model of titanium alloy laser cladding in open environment [J]. Chinese Journal of Lasers, 2020, 47(11): 1102006.
龚燕琪, 傅戈雁, 石拓, 等. 开放环境钛合金激光熔覆局部气氛保护模型研究[J]. 中国激光, 2020, 47(11): 1102006.
- [15] Wen H J, Meng X L, Xu X C, et al. Multi-objective optimization of laser cladding process parameters based on neural network and genetic algorithm [J]. Applied Laser, 2019, 39(5): 734-740.
温海骏, 孟小玲, 许向川, 等. 基于神经网络和遗传算法的激光熔覆工艺参数多目标优化[J]. 应用激光, 2019, 39(5): 734-740.
- [16] Zhang B, Chang S, Wang J, et al. Feature points

extraction of laser vision weld seam based on genetic algorithm [J]. Chinese Journal of Lasers, 2019, 46 (1): 0102001.

张斌, 常森, 王桔, 等. 基于遗传算法的激光视觉焊缝特征点提取 [J]. 中国激光, 2019, 46 (1): 0102001.

Parameter Optimization of High Deposition Rate Laser Cladding Based on the Response Surface Method and Genetic Neural Network Model

Pang Yifan, Fu Geyan*, Wang Mingyu, Gong Yanqi, Yu Siqu, Xu Jiachao, Liu Fan
Laser Manufacturing Technology Institute, School of Mechanical and Electrical Engineering, Soochow University, Suzhou, Jiangsu 215021, China

Abstract

Objective As a new advanced manufacturing technology, laser cladding rapid prototyping has been widely used to laser forming without any need for a mold or die. However, the traditional laser cladding usually adopts the low-power forming below 2000 W, which is inherent with problems such as low deposition efficiency, long-forming time, and insufficient material use. In contrast, the high-power hollow ring laser cladding can effectively improve the forming efficiency by optimizing the experimental process parameters using model analysis. In recent years, neural networks have been gradually applied to optimize multi-parameter objective in laser cladding, laser welding, and laser communication. The neural network prediction model is capable of fitting and modeling nonlinear data through iterative learning without the need to specify the function form in advance, demonstrating excellent ability to deal with multivariate nonlinear problems. However, the single neural network model may suffer from problems like slow and easy to fall into local extremum training speed. In this study, not only a neural network model optimized by a genetic algorithm is proposed to predict and optimize the laser cladding deposition efficiency, but also the parallel random search is employed to effectively solve the aforementioned two problems of the training process in the model. We expect that our research can contribute to improving deposition efficiency and shortening forming time in high-power laser cladding forming.

Methods The experimental equipment adopts the hollow ring internal light powder feeding cladding system, which mainly consists of a 6 kW Raycus laser, a 6-axis KUKA robot, and a hollow ring internal light powder feeding nozzle. The cladding material is Fe314 powder and the experimental substrate is 304 stainless steel. The effects of the laser power, scanning velocity, powder feeding velocity, and defocusing on the deposition rate of the cladding layer were studied systematically by an orthogonal experiment. The tissue differences of the samples under high and low deposition rates were consistently observed by scanning electron microscope. The Box-Behnken (BBD) experiment was then designed by the response surface method to study the influence of several interaction factors on the deposition rate. Meanwhile, the multiple regression model was also established to predict and optimize the deposition rate. Additionally, a series of randomized trials were conducted as a supplement. Both the results of the BBD experiment and the samples of the randomized trial were taken as the training data of the genetic neural network, and eventually, the genetic neural network model was trained to predict and optimize the deposition rate. By comparing the modeling ability, generalization ability, and optimization ability of the two models, the most suitable model was selected as the estimator for the following experiments to accomplish closed-loop control of the deposition rate.

Results and Discussions The range analysis method was adopted to analyze the orthogonal experimental results. It is indicated that powder feeding rate has the greatest influence on the cladding deposition rate followed by laser power and scanning speed, and the defocusing amount on the cladding deposition rate was of the least influence (Table 3). When it comes to the reciprocal influence of various factors on the deposition rate, the response surface methodology (RSM) model shows that the interaction effect between laser power and powder feeding rate is the most significant. This is probably because the laser energy density improves as the laser power enhances, resulting in the enlargement of the high-temperature range in the molten pool. Within a certain power range, the deposition rate

increases significantly by increasing the molten powder in the molten pool [Fig. 5(a)]. The second interaction effect is between scanning speed and powder feeding rate [Fig. 5(b)], and the interaction effect between defocusing amount and laser power is the least significant [Fig. 5(c)]. Simultaneously, the comparison of the predicted experimental values of genetic algorithms-back propagation (GA-BP) and RSM models after training shows that both models have good fitting accuracy, but the value of R^2 in GA-BP is closer to 1 (Fig. 8). By comparing the generalization ability of GA-BP and RSM models, the absolute average deviation(AAD) values of RSM and GA-BP models were 8.762% and 4.938%, respectively (Fig. 9). The maximum deposition rate obtained by the optimized GA-BP model was 61.74 g/min, which was higher than the value of 53.55 g/min obtained by the response surface method (Table 7). The above studies show that the prediction, generalization, and optimization capabilities of the genetic neural network model are superior to those of the response surface model, and the neural network model optimized by the genetic algorithm can provide a more effective prediction method for the achievement of laser cladding forming with high deposition rate.

Conclusions In this study, considering the orthogonal experiment in the hollow ring internal light powder feeding cladding system, the BBD experiment designed by response surface method was adopted and an RSM model using deposition rate as the response target was established. Subsequently, the influence of laser power, powder feeding speed, scanning rate, and defocusing amount on the deposition rate of high-power laser cladding was systematically investigated, individually or interactively. Based on the results of the BBD experiment and the samples of the randomized trial, a GA-BP model was set up. Comparing the performance of the two models by analyzing the modeling and generalization abilities, the technological parameters of laser cladding with high deposition rate were optimized. In conclusion, the performance of the GA-BP model is slightly better than that of the RSM model as the root mean square error and the average absolute deviation of the GA-BP model are smaller than those of the RSM model, and the decision coefficient values obtained in the RSM model and GA-BP model are 0.9479 and 0.9726, respectively. The prediction abilities of GA-BP and RSM models are fairly close, but under the condition of high deposition rate, the optimal deposition rate in the GA-BP model is 61.74 g/min, which is higher than the value of 53.55 g/min optimized by the RSM model. Briefly, the GA-BP model can be considered an effective method to optimize the high deposition rate of cladding. Because of the high reliability, the model can find the optimal deposition rate within a specific process range, which can be used as an estimator for operating closed-loop control over the following forming system to obtain high-efficiency and high deposition rate in the later cladding.

Key words laser processing; laser cladding; deposition rate optimization; response surface; genetic algorithm; neural network

OCIS codes 140.3390; 350.3850; 220.4610